TECTONICS, VOL. 6, NO. 6, PAGES 849-861, DECEMBER 1987

DETERMINATION OF THE TECTONIC STRESS TENSOR FROM SLIP ALONG FAULTS THAT OBEY THE COULOMB YIELD CONDITION

Ze'ev Reches

Department of Geology, Hebrew University,
Jerusalem

Abstract. A new method to calculate the stress tensor associated with slip along a population of faults is derived here. The method incorporates two constraints: First, the stresses in the slip direction satisfy the Coulomb yield criterion, and second, the slip occurs in the direction of maximum shear stress along the fault. The computations provide the complete stress tensor (normalized by the vertical stress), and evaluation of the mean coefficient of friction and the mean cohesion of the faults during the time of faulting. The present method is applied to three field cases: Dixie Valley, Nevada, Wadi Neqarot, Israel, and Yuli microearthquakes, Taiwan. It is shown that the coefficieet of friction of the three cases varies between $\mu < 0.1$ to $\mu = 0.8$. Further, it is demonstrated that previous stress inversion methods implicitly assume zero friction along the faults.

INTRODUCTION

The resolution of the state of stress associated with slip along a collection of faults, has been the goal of numerous studies since the work of Anderson [1942]. Some investigations of fault related stresses are based on the symmetry of the measured sets, the magnitude of the dihedral angle of the conjugate sets, utilization of known friction angles and assumed pore pressure [e.g., Zoback and Zoback, 1980]. Most faults are oblique slip and many fault populations cannot be separated into clear, symmetric sets. Therefore some investigations are based on determination of the strain axes of shortening and extension associated with the individual faults or the entire population [e.g., Arthaud, 1969; Reches, 1976; Aydin and Reches, 1980]. This approach is equivalent to the P-B-T axes analysis of focal plane solutions [Angelier, 1984].

Several stress inversion methods recently derived assume, following Bott [1959], that slip along a fault occurs in the direction of the resolved shear stress or, equivalently, normal to the direction of zero shear stress [e.g., Carey and Bruiner, 1974; Angelier, 1979, 1984; Armijo et al., 1982; Ellsworth, 1982; Gephart and Forsyth, 1984; Michael, 1984]. These methods determine the orientations of the principal stress axes which minimize the angular deviations between the observed slip direction along a fault and the direction of the maximum resolved shear stress determined from the calculated principal stress axes. However, the inversion "..method does not ensure that the observed fault planes are consistent with a reasonable failure criterion." [Gephart and Forsyth, 1984, p. 9314]. To overcome this inherent difficulty, Gephart and Forsyth [1984] and Michael [1984] determined the reduced stress tensor and then inspected whether the failure criterion is satisfied along each of the observed faults.

A new method to determine the state of stress associated with slip along faults is presented here. The analysis is based

Paper Number 7T0614.
0278-7407/87/007T-0614$10.00

on two constraints: First, the slip along a fault occurs in the direction of maximum shear stress (as in previous inversion methods), and second, the magnitudes of the shear and normal stresses on the fault satisfy the Coulomb yield criterion. This method provides the orientations and magnitudes of the principal stresses and constrains the coefficient of friction and the cohesion of the faults.

I present below the theory and method of computation, apply the method to three field cases and compare the present technique with previous methods.

THEORY

Approach

The objective is to determine the stress tensor which fits slip along all faults in a measured group. The method is based on the following assumptions:

1. The slip along a fault occurs in the direction of maximum shear stress or, equivalently, normal to the direction of zero shear stress (as in previous inversion methods).

2. The magnitudes of the shear and normal stresses on the fault satisfy the Coulomb yield criterion,

$$|\tau| > C + \mu \sigma_n \tag{1}$$

where τ is the magnitude of the shear stress in the slip direction, C is cohesion, μ is coefficient of friction and σ_n is the normal stress on the fault. No assumption is made about the age of the faults: They may be new faults, and then C is the cohesive strength of the intact rock and μ is the coefficient of internal friction, or they may be old, reactivated faults, and then C is the cohesive resistance to slip and μ is the coefficient of friction.

3. The slip event occurred under relatively uniform conditions: The cohesion and friction of the measured faults can be represented by their mean values, and the faults were active under a uniform state of stress.

The calculations provide a set of stress tensors, each one of them being the best fit tensor for a given coefficient of friction. The angle between observed and predicted slip axes is calculated and is regarded as an estimate of the degree of misfit of the solution. One selects the most suitable tensor by considering both a reasonable coefficient of friction and a low degree of misfit. The advantages of the procedure are demonstrated below.

Formulation

The known parameters for each fault are fault plane attitude, orientation of the slip axis and the sense of slip (normal or reverse). These parameters are represented by two unit vectors one normal to the fault N_i, i=1, 2 and 3, and the second parallel to the slip axis S_i, i=1, 2 and 3, where N_i and S_i are the directional cosines in an orthogonal coordinate system, X_i (Figure 1). In the present paper, X_1 points northward, X_2 points eastward, and X_3 points downward.

The geometric relations of directional cosines indicate that

$$\begin{aligned} N_1^2 + N_2^2 + N_3^2 &= 1 \\ S_1^2 + S_2^2 + S_3^2 &= 1 \\ N_1S_1 + N_2S_2 + N_3S_3 &= 0 \end{aligned} \tag{2}$$

The unknown stress components are $\sigma_{11}, \sigma_{22}, \sigma_{33}, \tau_{23}, \tau_{13}$, and τ_{12}.

Application of the Assumptions to the Known Parameters. Given S_i as the slip axis and B_i is the axis normal to it on the fault plane, then B = N x S, where x indicates vector multiplication. By following the stress analysis of Jeager and Cook [1969, chap. 2] and using the geometric relations of (2), assumption 1. becomes

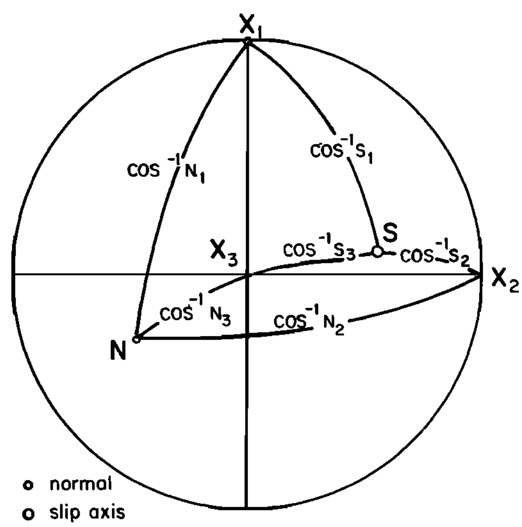

Fig. 1. Coordinate system and fault orientation data, stereographic projection, lower hemisphere. X_1 points northward, X_2 points eastward and X_3 points downward. N_i and S_i are the directional cosines of the normal to the fault and the slip axis.

$$(\sigma_{11} - \sigma_{33})N_1B_1 + (\sigma_{22} - \sigma_{33})N_2B_2 + \tau_{23}(N_2B_3 + B_2N_3) + \tau_{13}(N_1B_3 + B_1N_3) + \tau_{12}(N_1B_2 + B_1N_2) = 0, \quad (3)$$

and assumption 2. becomes

$$(\sigma_{11} - \sigma_{33})N_1S_1 + (\mu_{22} - \mu_{33})N_2S_2 + \mu_{23}(N_2S_3 + S_2N_3) + \tau_{13}(N_1S_3 + S_1N_3) + \tau_{12}(N_1S_2 + S_1N_2) \quad (4)$$
$$= C + \mu[(\sigma_{11} - \sigma_{33})N_1^2 + (\sigma_{22} - \sigma_{33})N_2^2 + \sigma_{33} + 2\tau_{23}N_2N_3 + 2\tau_{13}N_1N_3 + 2\tau_{12}N_1N_2].$$

Equation (1) appears here with an equality sign to facilitate the formulation of a system of linear equations.

By writing these two equations for each of the K faults in the studied set and after rearrangement of (4), one obtains a system of 2K equations. This system is the matrix multiplication A x D = F, where A is a 2K by 5 matrix, D is a vector of unknowns stresses with five terms and F is a vector with 2K terms. The matrix A has the form

$$[N_1B_1]_1 , [N_2B_2]_1 , [(N_2B_3 + B_2N_3)]_1 , [(N_1B_3 + B_1N_3)]_1 , [(N_1B_2 + B_1N_2)]_1$$
$$..... , ... , ... , ... , ...$$
$$[N_1B_1]_k , [N_2B_2]_k , [(N_2B_3 + B_2N_3)]_k , [(N_1B_3 + B_1N_3)]_k , [(N_1B_2 + B_1N_2)]_k \quad (5)$$
$$..... , ... , ... , ... , ...$$
$$[(N_1S_1 - \mu N_1^2)]_1 , [(N_2S_2 - \mu N_2^2)]_1 , [(N_2S_3 + S_2N_3 - 2\mu N_2N_3)]_1 , [(N_1S_3 + S_1N_3 - 2\mu N_1N_3)]_1 , [(N_1S_2 + S_1N_2 - 2\mu N_1N_2)]_1$$
$$..... , ... , ... , ... , ...$$
$$[(N_1S_1 - \mu N_1^2)]_k , [(N_2S_2 - \mu N_2^2)]_k , [(N_2S_3 + S_2N_3 - 2\mu N_2N_3)]_k , [(N_1S_3 + S_1N_3 - 2\mu N_1N_3)]_k , [(N_1S_2 + S_1N_2 - 2\mu N_1N_2)]_k$$
$$..... , ... , ... , ... , ...$$

where the subscripts 1 and k indicate the parameters associated with the first and k^{th} faults, and k ranges from 1 to K. The vector D of the unknown stresses has the form

$$(\sigma_{11} - \sigma_{33}),(\sigma_{22} - \sigma_{33}),\tau_{23},\tau_{13},\tau_{12} \quad (6)$$

The vector F has the form

$$0,0, ..,..,..,(C + \mu\sigma_{33}),(C + \mu\sigma_{33}),... \quad (7)$$

where the first K terms are zero and the last K terms are $(C + \mu\sigma_{33})$.

The system A x D = F is an overdetermined linear system in which A and F are known for the measured fault and slip orientations and the selected μ and C. The stress vector D can be determined by linear algebra methods. The magnitudes and orientations of the principal stresses, σ_1, σ_2 and σ_3, can be calculated from the stress tensor σ_{ij}.

Computation

The computation was accomplished in BASIC, using an IBM-PC computer. The main steps in the program are the following:

1. Selecting the coefficient of friction μ; I select a wide

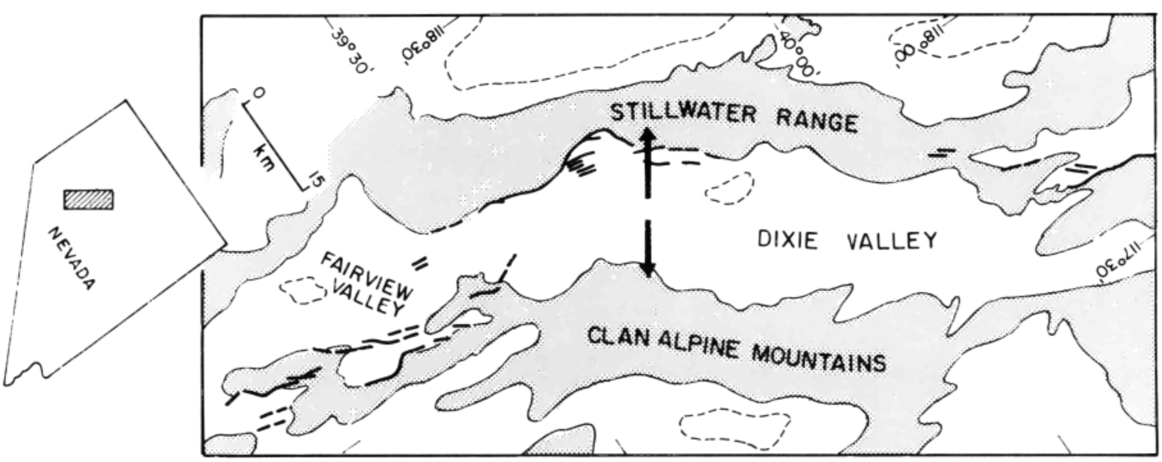

Fig. 2. Tectonic features in the Dixie Valley area, Nevada. Heavy solid lines indicate fault traces active in the 1903, 1915, and 1954 earthquakes [after Thompson and Burke, 1973]; heavy arrows indicate the orientation of σ_3, the least compressive stress axis calculated here (Table 1).

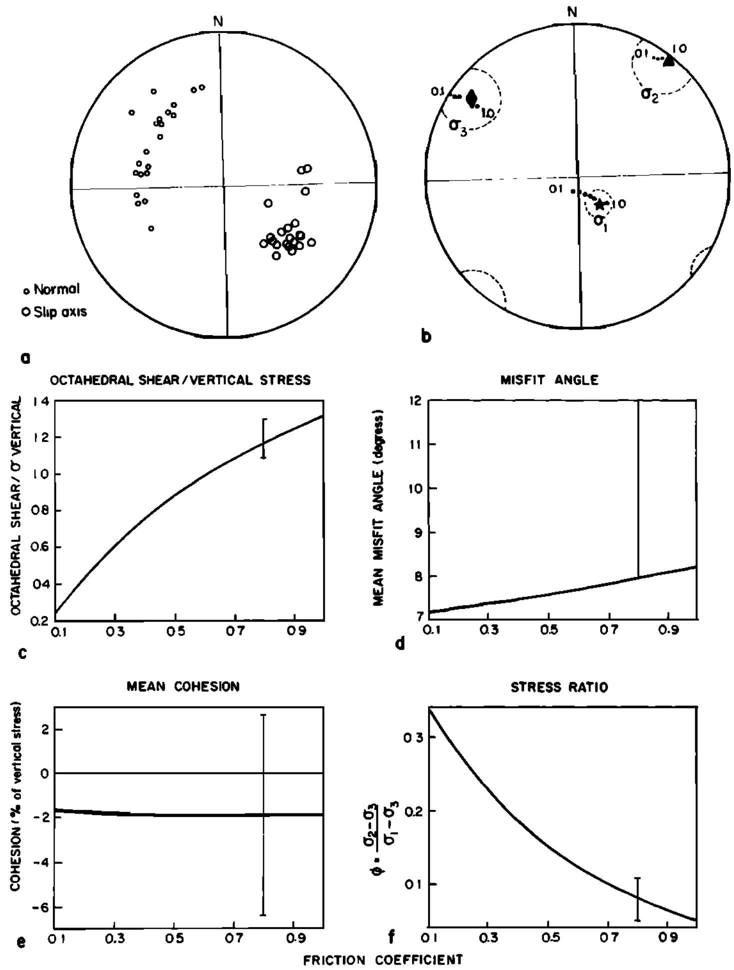

Fig. 3. Stress tensor analysis to a group of 22 faults in Dixie Valley, Nevada. Vertical bars in Figures 3c-3f for μ=0.8 indicate the standard deviations of the selected solutions. (a) Normals to faults and slip axes [after Thompson and Burke, 1973; Thompson, written communication, 1980]. Lower hemisphere, equal area projection. (b) Orientation of the three principal stress axes σ_1, σ_2 and σ_3, calculated in the present method for the marked coefficients of friction. Lower hemisphere, equal area projection. Solid symbols indicate the orientations of the principal stresses of the selected solution of μ=0.8: star for σ_1, triangle for σ_2 and rhomb for σ_3; the circles around the principal stress indicate the standard deviations of orientations of the principal stresses. (c) Normalized octahedral shear stress S_0 (equation (9)). (d) Mean misfit angle between observed and calculated slip axes of all faults. (e) Calculated mean cohesion (marked as fractions of σ_{33}). (f) Stress ratio as function of coefficient of friction.

range for friction: 0.01 < μ < 1.0. The mean cohesion is set as C=0.

2. Calculating the coefficients of matrix A (equation (5)) and vector F (equation (7)).

3. Solving the overdetermined system A x D = F for the five unknown stress components (the vertical stress σ_{33} scales the magnitudes of all other stresses). Following Schied [1968], the program determines the solution with the least squares method and provides the best fit tensor σ_{ij} and the mean square error RMS.

4. The six stress components are used to calculate the magnitudes and the orientations of the principal stresses σ_1, σ_2 and σ_3 [after Jaeger and Cook, 1969, chap. 2].

5. The stress tensor σ_{ij} is substituted into (4) for each fault. The program calculates for the k^{th} fault the normal stress, the shear stress in the slip direction, the cohesion $C_k = \tau_k - \mu (\sigma_n)_k$, and the misfit angle (the angle between the observed slip axis and the expected slip axis). The mean misfit angle and the mean cohesion are computed.

6. The results are displayed as plots of the octahedral shear

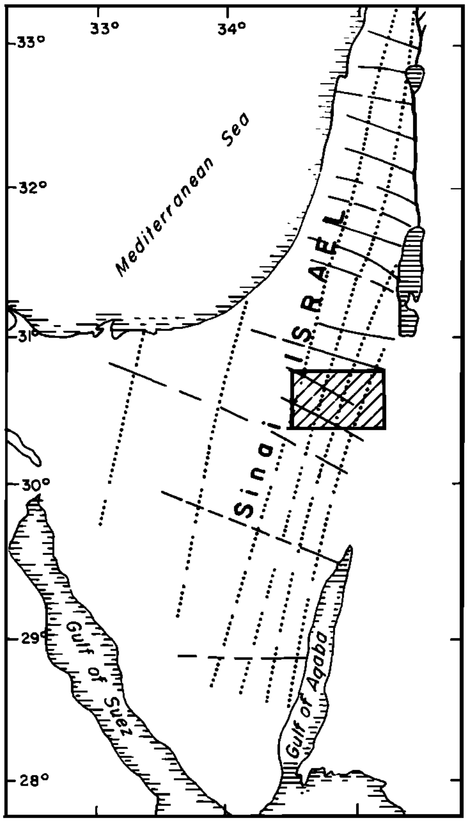

Fig. 4A. Simplified tectonic map of Sinai-Israel with the stress trajectories of the Syrian Arc stress field [after Eyal and Reches, 1983].

stresses, the mean misfit angle, the mean cohesion, the stress ratio, and the orientations of the principal stresses as functions of the coefficient of friction.

7. A Mohr diagram is plotted using the normal stress and the maximum shear stress calculated for the faults by the selected solution together with the assumed yield envelope and the Mohr circles. If the calculated slip direction along a fault is the inverse of the observed slip direction, this particular fault is excluded from the data set, and the computation is repeated.

8. The accuracy of the solutions is estimated from the mean square error.

FIELD EXAMPLES

The new method is applied to three cases: A set of 22 surfaces of normal faults with slip striations measured in Dixie Valley, Nevada [Thompson and Burke, 1973; Thompson, written communication, 1980] (Figures 2 and 3), a set of 16 right-lateral and left-lateral faults with slickensides measured in the Wadi Neqarot, southern Israel (Figures 4 and 5) [Eyal and Reches, 1983] and 17 faults with their 17 auxiliary planes determined from aftershocks of the Yuli earthquake, Taiwan (Figure 6) [Angelier, 1984].

Thompson and Burke [1973] studied the rate and direction of spreading at the Dixie Valley area, Nevada (Figures 2 and 3a). They determined a spreading direction of N55°W-S55°E from slickenside grooves on old faults in the bedrock, which is consistent with the spreading direction of the recent earthquakes. Zoback and Zoback [1980] showed that the slickenside grooves measured in Dixie Valley agree with the regional distribution of stress directions determined from earthquakes, hydrofracturing and fault slip data in north central Nevada.

Eyal and Reches [1983] determined the paleostress trajectories in Sinai-Israel subplate by analyzing the regional patterns of mesostructures. They detected two regional paleostress fields: One field is associated with the Syrian Arc

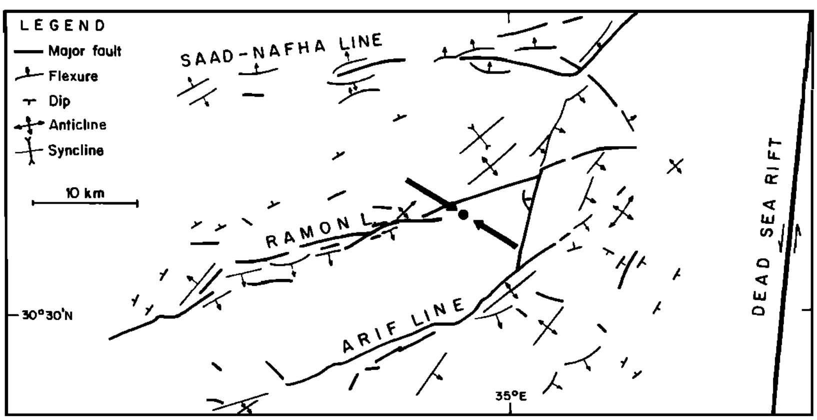

Fig. 4B. Tectonic features in the proximity of the Wadi Neqarot station [after Bartov, 1974].

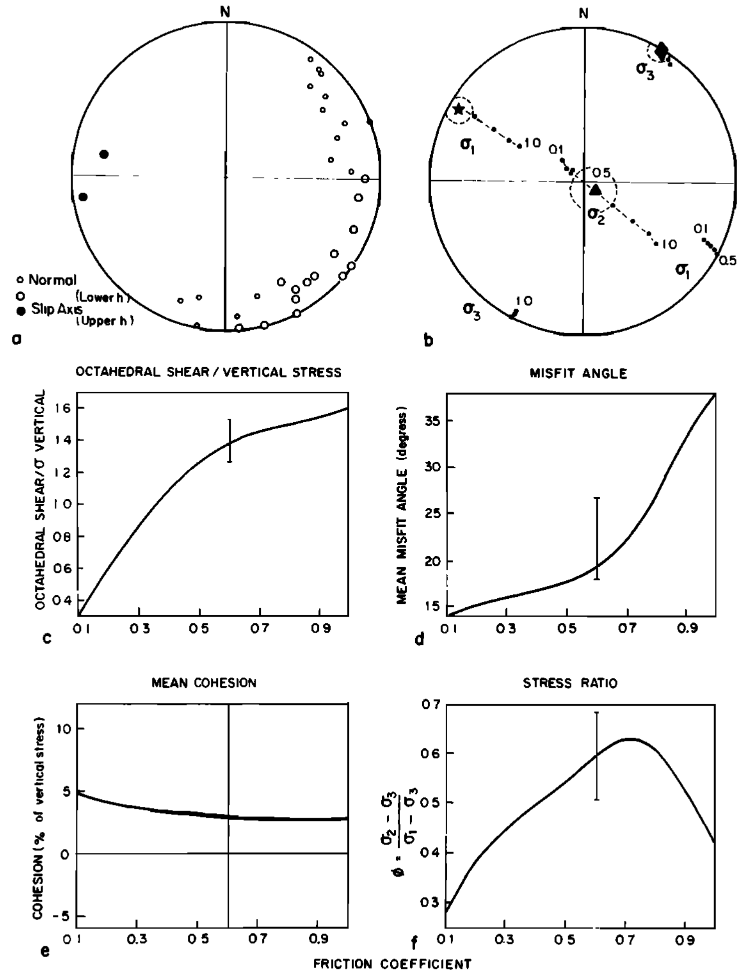

Fig. 5. Stress tensor analysis to a group of 16 faults in Wadi Neqarot, Israel. Vertical bars in Figures 5c-5f for μ=0.6 indicate the standard deviations of the selected solutions. (a) Normals to faults and slip axes [after Eyal and Reches, 1983]. Lower hemisphere, equal area projection. (b) Orientation of the three principal stress axes σ_1, σ_2 and σ_3, calculated in the present method for the marked coefficients of friction. Lower hemisphere, equal area projection. Solid symbols indicate the orientations of the principal stresses of the selected solution of μ=0.6: star for σ_1, triangle for σ_2 and rhomb for σ_3; the circles around the principal stress indicate the standard deviations of orientations of the principal stresses. (c) Normalized octahedral shear stress S_0 (equation (9)). (d) Mean misfit angle between observed and calculated slip axes of all faults. (e) Calculated mean cohesion (marked as fractions of σ_{33}). (f) Stress ratio as function of coefficient of friction.

deformation (Senonian to Miocene in age) (Figure 4A), and the second is associated with slip along the Dead Sea transform (Miocene to Recent in age). Eyal and Reches [1983] found that the paleostress fields are uniform and essentially independent of local structures. This observation is demonstrated here for one of their 130 stations, where 16 small wrench faults were measured in Cenomanian rocks in Wadi Neqarot, southern Israel (Figure 5a). This station is located within a complex region of faults, flexures, and domes of the Syrian Arc system, south of the Ramon structure (Figure 4B), yet the stress tensor determined for this station is in accord with the regional field (see below).

Seventeen focal plane solutions have been determined for aftershocks of Yuli earthquake in eastern Taiwan [Yu and Tsai, 1982]. Angelier [1984] cited their data and determined the reduced stress tensor for these focal solutions. The 17 focal

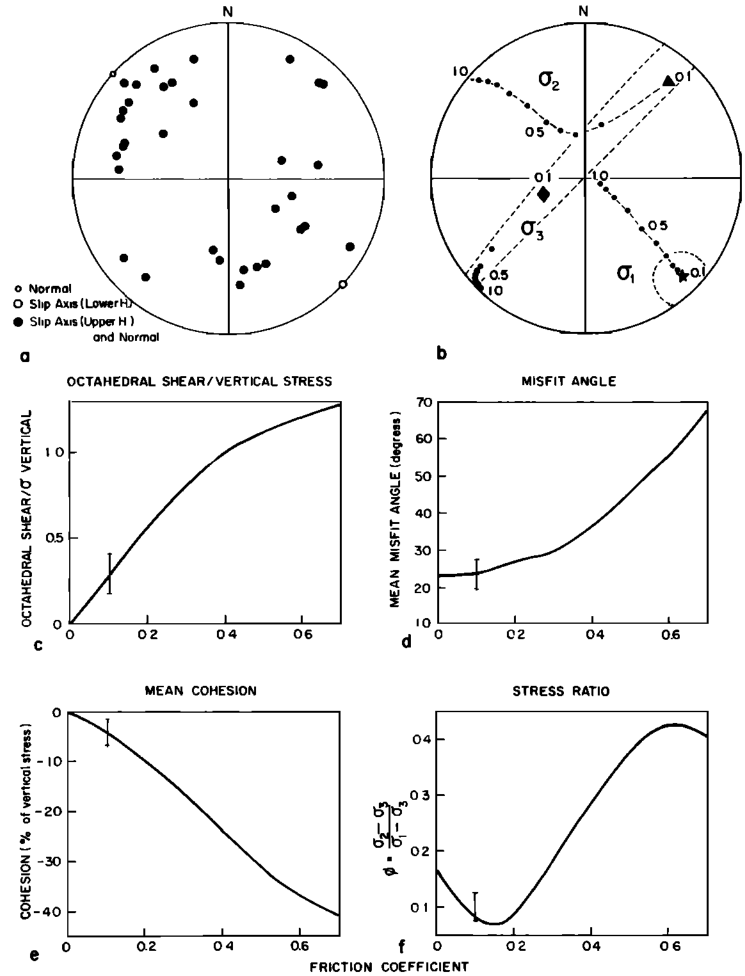

Fig. 6. Stress tensor analysis to a group of 17 faults and 17 auxiliary planes of microseismic events associated with Yuli earthquake, eastern Taiwan. Vertical bars in Figures 6c-6f for μ=0.1 indicate the standard deviations of the selected solutions. (a) Normals to faults and slip axes [after Angelier, 1984]. Lower hemisphere, equal area projection. (b) Orientation of the three principal stress axes σ_1, σ_2 and σ_3, calculated in the present method for the marked coefficients of friction. Lower hemisphere, equal area projection. Solid symbols indicate the orientations of the principal stresses of the selected solution of μ=0.8: star for S_1, triangle for S_2 and rhomb for S_3; the circles around the principal stress indicate the standard deviations of orientations of the principal stresses. (c) Normalized octahedral shear stress S_o (equation (9)). (d) Mean misfit angle between observed and calculated slip axes of all faults. (e) Calculated mean cohesion (marked as fractions of σ_{33}). (f) Stress ratio as function of coefficient of friction.

solutions provide the orientations of 17 fault planes and their 17 auxiliary planes. Twelve of the focal solutions indicate reverse slip, and five indicate oblique strike slip.

Parameter Investigation

The solutions for each case were calculated for $0.01 < \mu < 1.0$, vertical stress σ_{33}=1 (the scaling stress), and mean cohesion C=0. The solutions are presented by six diagrams which show the variations of the following parameters with the coefficient of friction:

1. The original fault slip data (Figures 3a, 5a and 6a).

2. The orientations of the principal stress axes (Figures 3b, 5b and 6b).

3. The normalized octahedral shear stress,

$$S_o=[(\sigma_1-\sigma_2)^2+(\sigma_2-\sigma_3)^2+(\sigma_3-\sigma_1)^2]^{1/2}/\sigma_{33} \qquad (9)$$

TABLE 1. Selected Solutions for the Three Field Examples

	Faults	Faults Friction	Mean Misfit[a]	Mean Cohesion[b]	Principal Stresses: Mean Magnitudes[b]			Principal Stresses: Orientations[c]			Stress Ratio
					σ_1	σ_2	σ_3	σ_1	σ_2	σ_3	
Dixie Valley	22	0.8	8	0.04	1.09	0.28	0.21	71/137	3/38	18/307	0.08
Wadi Neqarot	16	0.6	19	0.17	1.44	0.99	0.32	7/300	82/129	1/30	0.60
Yuli earthquakes	34	0.1	24	0.05	1.19	1.01	0.98	11/135	19/041	66/255	0.08

Dixie Valley, Thompson and Burke [1973].
Wadi Neqarot, Eyal and Reches [1983].
Yuli earthquakes, Angelier [1984].
[a] In degrees.
[b] Normalized by the vertical stress.
[c] Plunge (in degrees)/ Trend (in degrees).

which is a measure of the three dimensional stress differences (Figures 3c, 5c and 6c). S_0 increases monotonously and nonlinearly with μ in all three cases.

4. The mean misfit angle between observed and expected slip axes of the faults (Figures 3d, 5d and 6d). This angle increases nonlinearly with μ.

5. The calculated mean cohesion along the faults (Figures 3e, 5e and 6e).

6. The stress ratio (Figures 3f, 5f and 6f),

$$\varnothing = (\sigma_2 - \sigma_3) / (\sigma_1 - \sigma_3) \qquad (10)$$

This parameter has been used in previous stress determinations [e.g., Angelier, 1984; Michael 1984].

Selection of a Preferred Solution.

Figures 3, 5 and 6 present the solutions of the three field cases for $0.1 < \mu < 1.0$ and C=0, and one has to select a preferred solution from this range. A preferred solution includes three components: (1) The friction coefficient μ is as close as possible to $\mu \approx 0.8$ [Byerlee, 1978]. (2) The mean misfit angle is as small as possible. (3) The mean cohesion is slip resisting, $C \geq 0$.

Dixie Valley Faults. The faults of Dixie Valley display steady behavior: Orientations of the principal axes are stable (Figure 3b), the mean misfit angle is between 7° and 8° for all friction coefficients (Figure 3d), mean cohesion is slip resisting for all friction coefficients within the statistical confidence limits (Figure 3e), and all principal stresses are compressive. The steady behavior of the solutions reflects the simple and clear pattern of this group of faults (Figure 3a).

I select a solution with the commonly used friction coefficient, $\mu = 0.8$ [Byerlee, 1978]; this solution is marked in Figure 3b and listed in Table 1.

Wadi Neqarot Faults. The numerical solution for Wadi Neqarot faults differs from the solution for Dixie Valley faults. The axes of the principal stresses σ_1 and σ_2 rotate significantly with μ (Figure 5b): Axis μ_1 rotates from plunging 13° toward 115° for μ=0.1, to plunging 51° toward 299° for μ=1.0, axis σ_2 rotates in an inverted manner, whereas axis σ_3 maintains approximately the same orientation for all μ values. The mean cohesion is slip resisting for all friction values (Figure 5e). Misfit angles are relatively small (below 19°) for $\mu < 0.6$ and they increase faster for $\mu > 0.6$ (Figure 5d).

I select here $\mu = 0.6$ as the preferred solution (dark symbols in Figure 5b and Table 1), because the solutions for $\mu < 0.6$ fit the data better than solutions with $\mu > 0.6$ (as reflected by the smaller misfit angle in Figure 5d), and on the other hand,

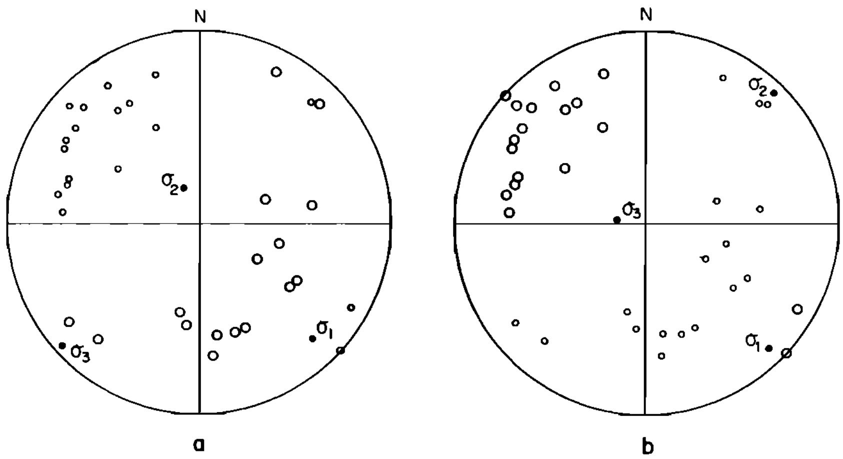

Fig. 7. Stress tensor solutions for two subsets (a and b), each with 17 planes of microseismic events associated with the Yuli earthquake, eastern Taiwan. Each figure includes the normals to faults, the slip axes, and the orientation of the three principal stress axes S_1, S_2, and S_3 for μ=0.1. Lower hemisphere, equal area projection. Data from Angelier [1984].

the coefficient of friction is relatively close to the experimental results of Byerlee [1978]. This process of somewhat "subjective" selection is discussed below.

Microseismic Events of Yuli Earthquake. Solutions were determined for three subsets of these events: all 34 planes, including faults and auxiliary planes, and two subsets each with 17 planes. I calculated the set of 34 planes for comparison with the results of Angelier [1984], and the other two subsets for investigation of the solution stability.

The solutions for the 34 planes of Yuli microearthquakes provide a restricted range for the preferred solution: The misfit angle is 24° for μ=0.1, 30° for μ=0.3, and increases faster for μ > 0.3 (Figure 6d). The solutions for μ > 0.05 yield negative mean cohesion, namely, slip supporting cohesion (Figure 6e); such solutions should be rejected. Thus both the relatively large misfit angle for μ > 0.1 and the negative cohesion for μ > 0.05 suggest that the preferred solution is in the range 0.0 < μ < 0.1. I select μ=0.1 (dark symbols in Figure 6b and Table 1) simply because I search for friction as large as possible.

The results for the other two subsets, each with 17 planes, are presented in Figure 7. The orientation of the σ_1 axis is similar in all three subsets (Figures 6b and 7), whereas they

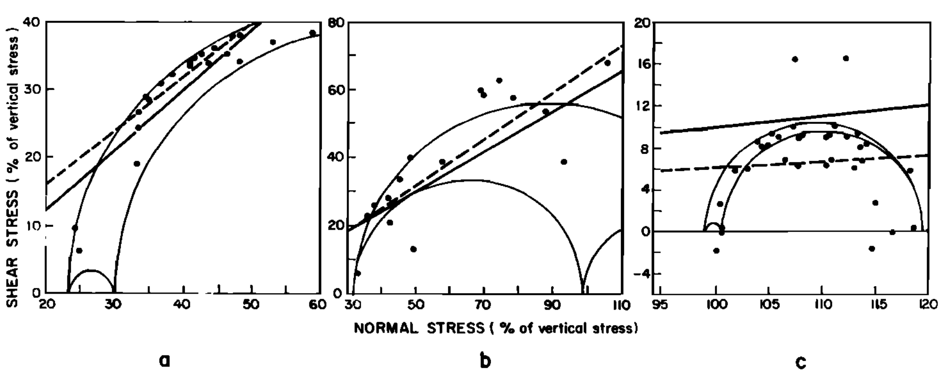

Fig. 8. Mohr diagrams of the selected solutions. Solid circles are the predicted maximum shear stress and the normal stress acting on each fault; the large circles are the Mohr circles of the determined principal stresses (Table 1); solid lines are the yield envelope $\tau = C + \mu\sigma_n$ used in the derivation (equation (7)); dashed lines are the linear regression yield envelope. (a) Dixie Valley faults, C=0 and μ=0.8. (b) Neqarot faults, C=0 and μ=0.6. (c) Yuli microearthquakes, C=0 and μ=0.1.

TABLE 2. Statistical Variations of the Selected Solutions

	Magnitudes[a]						Orientations[b]					
	σ_1	MD	σ_2	MD	σ_3	MD	σ_1	MD	σ_2	MD	σ_3	MD
Dixie Valley	1.09	.012	.28	.029	.23	.001	71/137	1.4	3/38	4.4	18/307	4.2
Wadi Neqarot	1.44	.002	.99	.037	.32	.06	7/300	1.2	82/129	4.2	1/30	4.1
Yuli quakes	1.19	.001	1.01	.021	.98	.019	11/135	1.3	19/041	62.7	66/255	62.7

MD, Maximum deviation from the best fit axis (as fraction of the vertical stress for magnitudes, and angles in degrees for the orientations)

[a] Normalized by the vertical stress.

[b] Plunge (in degrees)/ Trend (in degrees).

differ in the orientations of the σ_2 and σ_3 axes. The orientations of σ_2 and σ_3 interchange positions in a plane normal to the σ_1 axis (Figure 7).

The Yield Condition

The relations between the calculated stresses and the assumed Coulomb yield condition (equation (1)) is examined here.

Figure 8 displays Mohr diagrams of the selected solutions of the three field cases. It includes plots of the maximum shear stress versus the normal stress for each individual fault, Mohr circles for the best fit principal stresses, the yield envelopes used in the calculations ($\tau = 0.8\ \sigma_n$ for the Dixie Valley case, $\tau = 0.6\ \sigma_n$ for the Neqarot case and $\tau = 0.1\ \sigma_n$ for the Yuli earthquakes case) and the yield envelope calculated by linear regression for the shear and normal stresses.

Good agreement appears between calculated and expected yield conditions for Dixie Valley (Figure 8a) and Wadi Neqarot (Figure 8b), and only fair agreement appears for Yuli earthquakes (Figure 8c). The good agreement is apparent in the distribution of the calculated stresses (solid circles in Figures 8a and 8b) along the selected yield envelopes (solid lines in Figures 8a and 8b), the good correlation coefficients found in the linear regression calculations of the yield envelopes (dashed lines in Figures 8a and 8b), and the approximate tangential relationship between the Mohr circles and the yield envelopes. The agreement is only fair for the Yuli earthquakes where stresses for most faults are close to the yield envelopes (solid circles in Figure 8c) and the slope of the selected yield envelope, μ=0.1, is essentially the same as the slope of the regression envelope.

ACCURACY OF THE SOLUTIONS

The least squares solution of the overdetermined linear system provides the stress tensor (equation (6)), which minimizes the residual vector

$$R = A \times D - F$$

where A is a matrix calculated from the fault slip data (equation (5)), D is a vector of the components of the stress tensor (equation (6)) and F is a vector calculated from the vertical stress, friction, and cohesion (eq. 7). For a set of K faults the vector R has 2K terms, from r_1 to r_{2k}. The accuracy of the solution is represented by the root of the mean square error,

TABLE 3. Comparison of Present and Previous Results

	Mean Friction	Mean Misfit[a]	Orientations[b] σ_1	σ_3	Stress Ratio
Dixie Valley					
Selected solution (present)	0.8	7.8	71/137	18/307	0.08
Special solution (present)	0.01	7.0	81/224	1/123	0.39
Michael [1984]		5.6		to 124	0.48
Yuli earthquakes					
Selected solution (present)	0.1	24	11/135	66/255	0.08
Special solution (present)	0.01	23	9/135	77/276	0.16
Angelier [1984] (first)		30	5/121	82/249	0.2
Angelier [1984] (second)		26	2/131	81/028	0.0

[a] In degrees.
[b] Plunge (in degrees)/ Trend (in degrees).

$$RMS = \{ (\Sigma r^2_k) / 2K \}^{1/2}$$

where r_k is the residual of the k^{th} fault [Scheid, 1968, chap. 28]. The RMS is regarded as an estimate of the standard deviation of the best fit solution.

The magnitudes and orientations of the principal stress axes depend non linearly on F: The solutions for $F_1 = F + RMS$ and for $F_2 = F - RMS$ are not symmetrical with respect to the solution for F, and thus three sets of solutions are calculated, for F, F_1, and F_2, for the selected friction. The results of the three solutions are shown in Figures 3, 5, and 6 and listed in Table 2.

The deviations of the magnitudes of the principal stresses ranges from 1% to 17% of the vertical stress σ_{33}, with mean deviation of 5.8% (Table 2). Thus the magnitudes of the principal stresses of the best fit solutions are good estimates of the "true" magnitudes in the three field cases.

The angular deviations of the axes orientations of Dixie Valley and Wadi Neqarot range from 7.7° to 20.9° (Table 2 and Figures 3b and 5b). For the Yuli microearthquakes case, the angular deviations for σ_1 axis are up to 15.2°, and σ_2 and σ_3 interchange their positions in a plane normal to σ_1 (Figure 6b). This interchange of stress axes is also reflected in the essentially identical magnitudes of σ_2 and σ_3 (Table 2) and in the solutions for the two subsets of this group (Figure 7). Thus, $\sigma_2 \approx \sigma_3$ for the case of Yuli earthquakes, and $\emptyset \approx 0$.

Figures 3e and 5e indicate that the mean cohesion for Dixie Valley and Wadi Neqarot may be regarded as zero, in agreement with the initial selected cohesion. Further, it appears that the mean cohesion in these cases hardly depends on the friction coefficients (Figures 3e and 5e). The mean cohesion of the Yuli earthquakes for μ=0.1 is slightly negative, $C = (-0.042 \pm 0.027)\sigma_{33}$ (Figure 6e). The difference between this value and the initial cohesion C=0 suggests that a better solution for the Yuli earthquakes should probably be with $\mu < 0.05$.

DISCUSSION

Comparison with Previous Methods

Two of the field examples were analyzed previously, Dixie Valley by Michael [1984] and Yuli earthquakes by Angelier [1984]. Table 3 lists the previous results, the selected solutions of the present method and solutions of the present method for μ=0.01.

As in the present study, Michael [1984] assumed that the resistance to slip along the faults can be represented by a mean cohesion and a mean friction coefficient. His formulation, which is based on the assumptions of uniform shear stress along the slipping faults, is similar to the present formulation (compare equations 3 and 4 of Michael, 1984, with present (5) and (6)). The results of Michael for the Dixie Valley case are in agreement with the results of the solution for μ=0.01 (Table 3). The agreement is good for the orientations of the principal stresses [see also Figure 4 in the work by Michael, 1984] and the angle of misfit, and fair for the stress ratio (Table 3). Michael's results are only roughly similar to the selected solution of the present method for μ=0.8 (Tables 2 and 3).

Angelier [1984] calculated the reduced stress tensor for the focal solutions of the Yuli microearthquakes by using his inversion techniques. His results, including the orientations of the principal stresses, the stress ratio Ø and the angle of misfit, are in good agreement with the solution of the present method for μ=0.01 (Table 3).

The inversion methods of Angelier and Michael do not consider the friction coefficient and the cohesion and they provide a single, special solution. On the other hand, the present method provides a collection of permissible solutions. The good agreement found between the present solutions for μ=0.01 (solution for μ=0 is not permitted for numerical reasons) and the results of the previous methods suggests that these solutions implicitly consider the case of μ=0. This suggestion is expected. Previous methods minimize the angle of misfit, and, as demonstrated here, the smallest angle of misfit is indeed for μ=0 (Figures 3d, 5d and 6d).

Solution Selection Procedure

While applying the present method to field cases I searched for solutions which include coefficients of friction as close as possible to measured rock friction and relatively small angles of misfit. This apparently "subjective" selection procedure indicates the utilization of two independent constraints: the yield criterion and the slip in maximum slip direction.

One may use an "objective" selection procedure which is based on one constraint, for example, minimizing the angle of misfit (similarly to Gephart and Forsyth [1984], Angelier [1984] and Michael [1984]). However, minimizing the angle of misfit provides no control on the friction coefficient, and in the present field examples it would lead to nonrealistic solutions of μ=0 (Figures 3, 5 and 6). Therefore the selected solution reflects the choice between two options: smallest misfit angle with a nonrealistic zero friction or somewhat larger misfit angle with reasonable friction coefficient. I prefer the second.

CONCLUSIONS

The present method incorporates a yield criterion and the concept that slip occurs in the direction of maximum resolved shear on a fault plane. The computations provide several permissible stress solutions, and the selection of the most suitable solution is based on field observations and mechanical considerations. Furthermore, one obtains the mean coefficient of friction and the mean cohesion which best fit slip along all faults in the given group. The method also determines the magnitudes of the three principal stresses (in relation to the vertical stress). As the absolute magnitude of the vertical stress may be estimated from depth of faulting, the new method yields the absolute magnitude of the tectonic stress tensor.

The stress tensor determined here for Dixie Valley (Table 1) is in good agreement with the local fault pattern (Figure 2) and it fits local and regional extension directions of central Nevada [Thompson and Burke, 1973; Zoback and Zoback, 1980]. Similarly, the stress tensor of Wadi Neqarot (Table 1) fits the regional Syrian Arc deformation of the Sinai-Israel subplate (Figure 4) [Eyal & Reches, 1983]. Furthermore, the present method provides results similar to the stress inversion results of Michael [1984] (Dixie Valley faults) and Angelier [1984] (Yuli Microearthquakes). However, the results are in good agreement only when the present method considers $\mu \approx 0$, thus suggesting that previous techniques are valid for cases of very low coefficient of friction.

Future improvement of the method will incorporate variations in the pore-fluid pressure and consideration of non uniform cohesion and friction.

Acknowledgements. This study was initiated a few years ago when Atilla Aydin and I tried to resolve the state of stress associated with faulting from strain considerations and symmetry arguments. The study with Atilla Aydin and stimulating discussions with Paul Delaney significantly contributed to the present work. George Thompson kindly provided some of his and Dennis Burke's unpublished data on faults in Dixie Valley, Nevada. John Gephart, Andy Michael and an annonymous critic reviewed the manuscript and made many helpful comments. I benefited from conversations with John Gephart, Mary-Lou Zoback, Marie Jackson-Delaney and Jacques Angelier. The study was supported by a grant from the Central Research Fund of the Hebrew University, Jerusalem.

REFERENCES

Anderson, E. M., *The Dynamics of Faulting*, 183 pp., Oliver and Boyd, London, 1942.

Angelier, J., Determination of the mean principal directions of stresses for a given fault population, *Tectonophysics, 56*, T17-T26, 1979.

Angelier, J., Tectonic analysis of fault slip data sets, *J. Geophys. Res., 89*, 5835-5848, 1984.

Armijo, R., E. Carey, and A. Cisternas, The inverse problem in microtectonics and the separation of tectonic phases, *Tectonophysics, 82*, 145-160, 1982.

Arthaud, F., Methode de determination graphique des directions deraccourcissement, d'allongement et intermediare d'une population de failles, *Bull. Soc. Geol. Fr.*, *7*, 729-737, 1969.

Aydin, A., and Z. Reches, Determination of the orientation of the principal stresses from three or more sets of contemporaneous faults (abstract), *EOS Trans. AGU*, *61*, 1117, 1980.

Bott, M. H. P., The mechanics of oblique slip faulting, *Geol. Mag.*, *96*, 109-117, 1959.

Byerlee, J. D., Friction of rocks, *Pure Appl. Geopgy.*, *116*, 615-626, 1978.

Carey, E., and B. Bruiner, Analyse theorique et numerique d'un modele mechanique elementaire applique a l'etude d'une population de failles, *C. R. Hebd. Seances. Acad. Sci. Ser. D*, *279*, 891-894, 1974.

Ellsworth, W.L., A general theory for determining the state of stress in the earth from fault slip measurements, *Terra Cognita*, 2(2), 170, 1982.

Eyal, Y. and Z. Reches, Tectonic analysis of the Dead Sea Rift region since the Late-Cretaceous based on mesostructures, *Tectonophysics*, *2*, 167-185, 1983.

Gephart, J. W., and D. W. Forsyth, An improved method for determining the regional stress tensor using earthquake focal mechanism data: Application to the San Fernando earthquake sequence, *J. Geophys. Res.*, *89*, 9305-9320, 1984.

Jaeger, J. C. and N. W. G. Cook, *Fundamentals of Rock Mechanics*, 513 pp., Methuen, London, 1969.

Michael, A. J., Determination of stress from slip data: Faults and folds, *J. Geophys. Res.*, *89*, 11,517-11,526, 1984.

Reches, Z., Analysis of joints in two monoclines in Israel, *Geol. Soc. Am. Bull.*, *87*, 1654-1662, 1976.

Schied, F., *Numerical Analysis, Schaum's Outline Ser.*, 422 pp., McGraw-Hill, New York, 1968.

Thompson, G. A. and D. B. Burke, Rate and direction of spreading in Dixie Valley, Basin and Range Province, Nevada, *Geol. Soc. Am. Bull.*, *84*, 627- 632, 1973.

Zoback, M. L., and M. D. Zoback, Faulting patterns in north-central Nevada and strength of the crust, *J. Geophys. Res.*, *85*, 275-284, 1980.

Z. Reches, Department of Geology, Hebrew University, Jerusalem, 91904, Israel.

(Received December 22, 1986;
revised July 13, 1987;
accepted July 17, 1987)